Response to Review Comments (Referee #2)

Manuscript ESSD-2026-299

"An Ensemble Dataset of Permafrost Thaw Conditions for Northern High Latitudes Using Open Satellite Data"

Dear Referee #2,

Thank you for your valuable comments. Please find below our point-by-point responses and the corresponding revisions. Upon the ESSD review procedure, the final revised manuscript will be provided after the review window is closed.

In summary, the revised manuscript includes the following major changes:

- **An extensive search for permafrost monitoring stations for validation:** The borehole sites increased from 26 from one network to 96 sites from four networks.
- **Two new figures:** One shows the spatial patterns of ΔPP and ΔMAGT of the three published products (Obu, NIEER, Permafrost_CCI) relative to the ensemble product. The other shows the distribution of expanded 96 borehole sites and presents the updated scatterplot.
- **Two new subsections**: 3.1.3 "Spatial uncertainties in satellite-based permafrost products"; and 3.3.3 "Model performance and comparison with borehole records".
- **Expanded discussion:** Section 3.4 "Satellite-based open data for permafrost research" was expanded.
- **12 new references** relevant to our revision were added.

The editorial comment regarding the online visibility of Table 4 was also addressed. The gray shading was removed and replaced with a bold border.

1. Uncertainty

It should be taken into account to which extent the input data sets provide uncertainty layers together with the data, how this differs in time and space, which regions may be specifically vulnerable to compounded errors and how this carries on in the created ensemble. The current extent of discussion of inherent uncertainties is not sufficient.

This is an excellent point that was also raised by other reviewers. We made substantial revisions to address the uncertainty issue.

(1) We elaborated on the spatial variations among the three published permafrost maps, and added a new figure (Fig.5) to the revised manuscript.

Specifically, a new subsection, "**3.1.3 Spatial uncertainties in satellite-based permafrost products**" was added to the **Results** section. This subsection examines the spatial patterns of prediction errors among the three permafrost products relative to our ensemble product, as quantified by ΔPP and ΔMAGT. This new analysis also addresses a comment from Dr. Way. A new figure was added to facilitate visual comparison. For your reference, we provide the revised text and figure below.

"*The differences in PP and MAGT of the three permafrost products (source maps) relative to the ensemble product are spatially compared in Fig.5. For PP, all three source maps (Fig.5a-5c) show strong agreement with the ensemble product in the interior of the study region, corresponding to areas of continuous permafrost (PP=100%). Greater discrepancies occur farther south, in areas characterized by discontinuous, sporadic and isolated permafrost. Overall, the hot and cold spots of PP difference are localized, occurring as small patches in local areas. One notable example is the Permafrost_CCI PP map, which exhibits substantial overestimation along the southern margin of Siberia in northern Asia (red patches in Fig.5c). Moreover, all three source maps indicate a more northerly permafrost limit than that delineated by the IPA map that is shown as the background layer. This is consistent with findings reported in previous studies and may be attributed two factors: (1) satellite-based products capture finer spatial details than the IPA map that was developed largely based on expert knowledge; and (2) permafrost retreat since the publication of the IPA map that may date back to the 1950s in some regions. Our ensemble PP product provided an updated baseline representation of permafrost distribution while reducing the influence of uncertainties associated with individual source maps.*

For MAGT, the three source maps also exhibit notable regional differences in their spatial patterns. For example, in central Siberia, the Obu map (Fig.5d) shows substantial underestimation relative to the ensemble product, whereas the NIEER map (Fig.5e) contains a concentrated cluster of strong overestimation. The Permafrost_CCI map (Fig.5f) displays several localized hot spots in northern Asia and cold spots in the High Arctic of northern Canada. By taking the median values from the three maps, our ensemble MAGT product reduced these region-specific uncertainties and biases associated with individual MAGT maps, thereby providing a more robust representation of permafrost thermal conditions across the northern high latitudes."

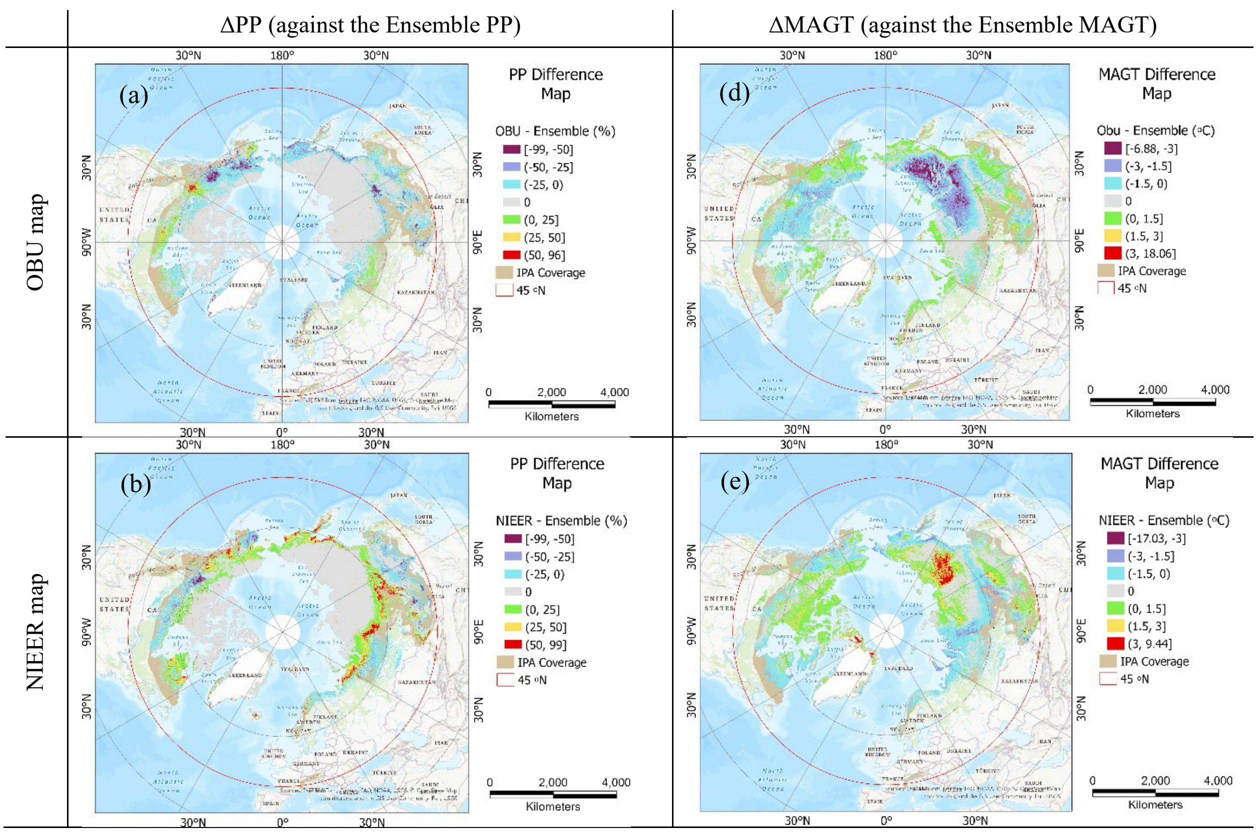

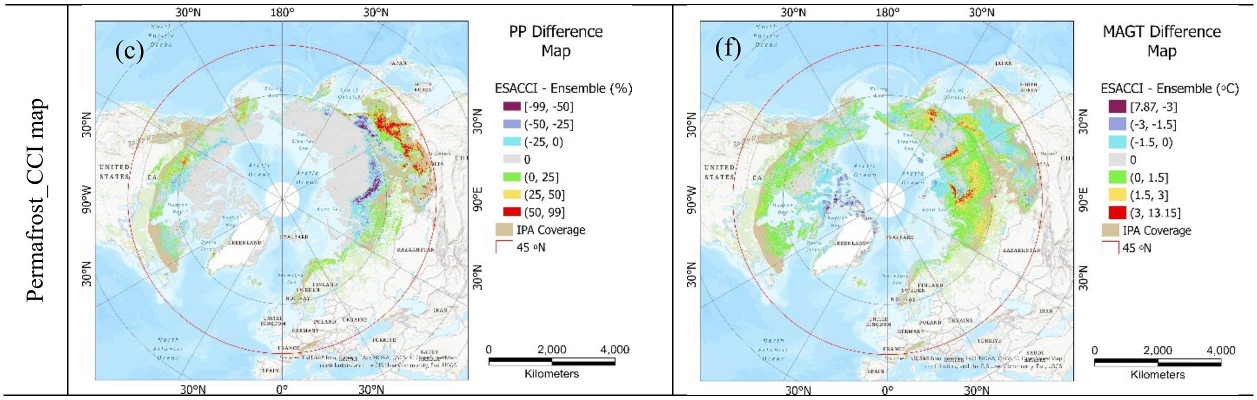

Figure 5 Spatial differences of the three source maps (Obu, NIEER, Permafrost_CCI) relative to the ensemble product. The left panels (a–c) are the PP differences, and the right panels (d–f) are the MAGT differences. Areas in light gray (zero difference) represent locations where the ensemble value is selected. The light brown background outlines the IPA permafrost map.

(2) We strengthened the uncertainty assessment of the predicted PTI map by collecting additional borehole records through extensive search of permafrost monitoring networks and recently released datasets in 2025, bringing the total to 96 borehole sites. This expanded validation set enabled a more robust comparison between the predicted and station-derived PTI values.

In summary, we identified four network and dataset sources relevant to our study: the Nordicana D Network, the Swiss PERMOS Network, a European open-source dataset, and the expanded GTN-P and CALM databases released through PANGARA last year. In total, 96 borehole sites were compiled across the study region for validation.

We substantially expanded **Subsection 3.3.3** and renamed it "**3.3.3 Model performance and comparison with borehole records**". Figure 10 was also revised to include two panels: a map showing the distribution of all borehole sites (Fig.10a) and an updated scatterplot (Fig.10b). With the inclusion of a much larger in-situ dataset, the Spearman' r increased from 0.69 to 0.84, indicating stronger agreement between the borehole observations and the predicted PTI values.

The complete revision is copied here for your reference:

"…This study searched all publicly available permafrost station networks to access those valuable observational records. To ensure a consistent representation of mean MAGT and MAGT|ALT trends, only stations with both MAGT and ALT records spanning at least three years were included in the analysis. Stations with only one of the two permafrost variables available were excluded.

Globally, two major worldwide networks are available for monitoring permafrost conditions and changes: the Global Terrestrial Network for Permafrost (GTN-P, 2018; GTN-P, 2021) and the Circumpolar Active Layer Monitoring (CALM) program (Nelson et al., 2021). GTN-P was established by IPA in 1980 and currently involves 33 countries, with 1,487 permafrost-temperature sites and 256 active-layer-thickness sites using boreholes at various depths from 0 – 20 m. CALM was established in 1991 in a voluntary basis and currently involves 15 countries, monitoring more than 125 sites, approximately 60 of which measure ALT on grids ranging from 1 ha to 1 km^2. In 2025, GTN-P MAGT and CALM ALT datasets for the Northern Hemisphere were released through PANGARA (Wieczorek et al. 2025; Streletskiy et al. 2025), although the periods of record vary among sites, and GTN-P and CALM monitoring sites are often not geographically co-located. All stations located in the northern high latitudes (> 45ºN) were examined in this study. The two measurements were paired when the GTN-P and CALM sites were geographically close (while the collection years often vary). A total of 57 paired GTN-P/CALM stations were identified from the 2025 datasets. The distances between the paired GTN-

P and CALM sites range from 0 to 47.02 km. For these stations, the annual MAGT and ALT values were obtained, from which the mean MAGT and both trends of MAGT and ALT were calculated.

The GTN-P and CALM stations are operated by national and regional monitoring programs, through which additional ground-temperature measurements at more stations have been collected. Although MAGT and ALT records are not always directly available as for the GTN-P/CALM stations, many of these borehole sites are equipped with thermistor cables that record ground temperatures at multiple depths in a daily or finer interval. Using these vertical borehole temperature profiles, we derived annual MAGT and ALT values as described below. MAGT was defined as the mean annual ground temperature at the depth of zero annual temperature amplitude. For each site, we examined its daily temperature profiles to identify this depth, which was approximated as the depth at which the difference between the maximum and minimum daily temperatures over a year was less than 0.15 °C. When no measurement depth satisfied this criterion, the deepest available measurement depth was used as a proxy for the zero-amplitude depth. Some stations only release monthly temperature profiles, which may result in larger uncertainties in the calculation. ALT was determined as the annual maximum depth of the 0°C isotherm, calculated by linear interpolation between measurement depths that bracketed the 0 °C isotherm within each daily thermal profile. Only days on which the shallowest sensor recorded a temperature above 0 °C and a positive-to-negative temperature crossing with depth was present were considered valid. The maximum interpolated depth of the 0 °C isotherm among all valid days within a year was taken as the annual ALT. Once the annual MAGT and ALT values were extracted for each site, the mean MAGT and both trends of MAGT and ALT were calculated.

Three regional monitoring networks were identified during the course of this study, providing additional 39 stations with paired MAGT and ALT:

1) *Nordicana D Network, 2010-2022*

   The Nordicana D8 SILA (Borehole and Near-Surface Ground Temperature) Network comprises 46 boreholes across the Nunavik–Nunavut region of Canada (Allard et al., 2024). Each thermistor-equipped borehole records ground temperature at multiple depths from 3 to 20 m, with data available at four temporal resolutions (hourly, daily, monthly, yearly). We utilized the daily records to extract the MAGT and ALT values. Among all boreholes in this network, only 19 provided temperature time series that met our data requirements. The remaining sites were excluded because of insufficient borehole depth, significant data loss, or anomalous records in daily temperature profiles.

2) *Swiss Permafrost Monitoring Network (PERMOS), 1997-2024*

   Published by the Swiss Permafrost Monitoring Network, this database contains a series of permafrost variables at established borehole sites in the Swiss Alps mountains (PERMOS 2025). Our study utilized its daily ground-temperature time series recorded by borehole thermistors. The database contains 23 borehole sites in Alps permafrost regions. The PERMOS sites are spatially clustered, with multiple boreholes often established within 1 km of one another. Some boreholes have been included in the GTN-P network. In this case, to avoid spatial redundancy and duplication, we selected the borehole with the longest record to best represent permafrost conditions. After data screening, 10 borehole sites were retained. We extracted their annual MAGT and ALT values following the procedure described above.

3) *Open-source European mountain permafrost ground temperature dataset (Noetzli et al. 2024a), 1996-2022*

   Noetzli et al. (2024b) compiled a ground-temperature dataset from 64 boreholes located within or near European mountain permafrost regions, with observations collected from multiple national permafrost observation networks and institutions. The study reported a warming rate at a depth of 10 m exceeding 1 °C per decade in the region, suggesting accelerated ground warming and permafrost thaw in European mountains. Only monthly ground-temperature records are provided in this European open-

source dataset. Among the 38 boreholes located within our study region, some sites are from established networks such as PERMOS and GTN-P, while some boreholes are located too close to each other (< 1 km). Because only monthly temperature profiles are available, accurately calculating the depth of zero annual amplitude is challenging. In the European Alps as observed in the PERMOS database, the borehole depths are mostly 10 or 20 m and the depth of zero annual amplitudes is commonly near the deepest borehole measurement point. Following this observation, we approximated MAGT for each site in the European open-source dataset as the 12-month average of ground temperatures at the deepest available depth. ALT values were obtained from nearby CALM stations. The distances between the ground-temperature site and CALM site ranged from 0 to 41.77 km. After removing duplicate or closely spaced sites, 10 boreholes with data of sufficient quality were retained for our analysis.

From these global and regional networks, 96 stations with valid borehole records were retained for quality assessment of the predicted PTI map (Fig.10). Fig.10a displays their spatial distributions across the permafrost basemap, with a minimum distance of 1 km between any two stations. The PTI ranks at these stations were extracted using the same ranking system as presented in Table 3. Their PTI ranks ranged from 11 to 33 because borehole records did not consider Rank 40. For stations with Rank 33 but located within the isolated patches delineated by the IPA map, the PTI rank was re-assigned to 40. In the scatterplot of the station-extracted PTI and the predicted PTI (Fig.10b), the PTI at 40 out of 96 points matched exactly (lying on the 1:1 line) and 25 points differed by only one rank (close to the 1:1 line). The comparisons in Fig.10b yield a ranked correlation coefficient (Spearman's r) of 0.84, which is statistically significant based on a student's t test ($p < 0.001$). The strong goodness of fit indicates the validity of the predicted PTI map for assessing permafrost thaw conditions of permafrost in the study region. Three stations, as marked in Fig.10b, exhibited the largest discrepancies between the station-measured and predicted PTI values.

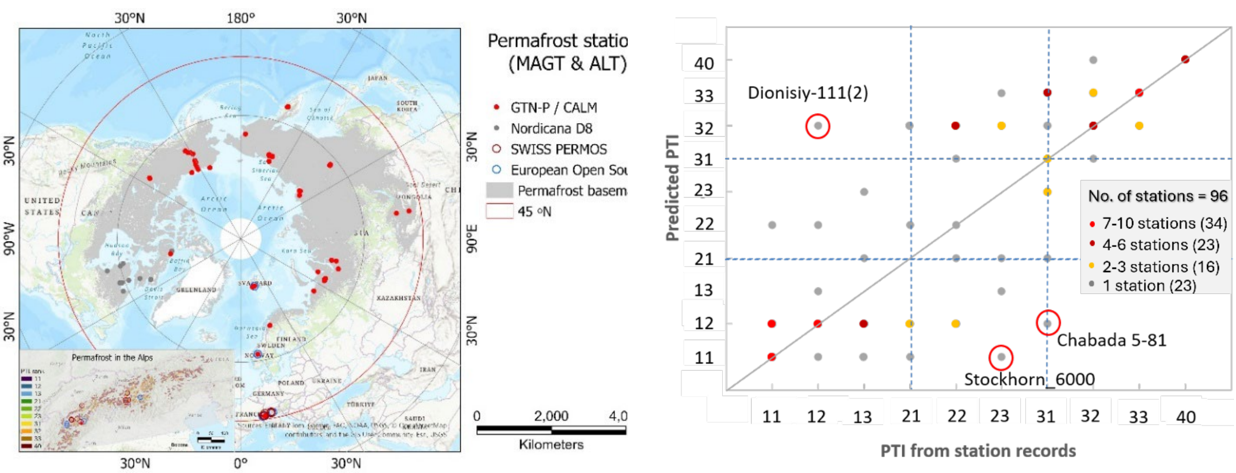

(a) *(b)*

Figure 10 Borehole sites used for quality assessment of the predicted PTI (a) and scatterplot comparing the borehole-derived and predicted PTI values (b). The inset in (a) shows the borehole sites in the Alps overlaid on the PTI map. Coloured dots in (b) indicate multiple stations.

Two stations revealed substantial underestimation of permafrost thaw by the predicted PTI. Chabada 5-81, registered as GTN-P #1115, had a station-derived PTI rank of 31, compared with a predicted PTI rank of 12. The station lies in a low-elevation, flat alluvial plain of the Lena River near Yakutsk, Russia. In the 2025 GTN-P database, this borehole has a long 36-year monthly record (1982–2018) with an average MAGT of -0.597 °C and no apparent trends on either MAGT or ALT. It is noteworthy that a nearby station, Chabada 8-82 (GTN-P #0950), is located only 4 km to the northeast. This station had a similar observation period but a substantially lower MAGT of -2.523 °C, also without apparent *trends on MAGT or ALT, resulting in a station-measured PTI rank of 21. This rank is more consistent with the predicted PTI rank of 12. Based on the environmental maps, both stations are situated within the extensive Lena River Floodplain, characterized by relatively homogeneous, deciduous coniferous forest within the East Siberian taiga. The predicted PTI map (Fig.9a) similarly shows an extensive homogeneous area classified as Rank 12. Therefore, although the model underestimated thaw conditions at Chabada 5-81, the predicted PTI appears to reasonably represent the broader regional pattern of permafrost thermal conditions.*

In contrast to the Chabada stations, Stockhorn_6000 from the European open-source dataset represents alpine permafrost at an elevation of 3,410 m in the Swiss Alps. Based on its 20-year monthly records (2001-2022), we calculated an average MAGT of -2.428 °C with trends observed on both variables (PTI = 23). These observations are generally consistent with other borehole records in this region. The predicted PTI, however, identified a small patch of PTI Rank 11 at the location of this station. As shown in the inset of Fig.10a, permafrost in the Alps is distributed at high elevations and is characterized by greater thaw potential (predicted PTI ranks 32–40). The surrounding ecoregion is European-Mediterranean montane forest, with dominant land covers ranging from grasslands to barren tundra and glaciers. This station is located within a transition zone of barren tundra and glacier, which may attribute to the discrepancy between the borehole-derived and satellite predictions. Further investigation using localized, fine-scale environmental data is needed to determine where such extremely isolated patches of highly stable permafrost are present, or whether the discrepancy reflects limitations in the spatial resolution of satellite open data.

One station revealed a substantial overestimation of thaw. Dionisiy-111(2), recognized as GTN-P #1710, is located on the Chkotka Peninsula in northeastern Russia. The Arctic peninsula is predominantly covered by herbaceous and low shrub tundra within the Bering tundra ecoregion. The borehole site is situated on an isolated massif of Mount Dionisiy rising above the surrounding Anadyr lowland. Based on its 26-year annual records (1987-2012), the site had an average MAGT of -4.0 °C with increasing MAGT trend but no ALT trend. Its station-derived PTI was 12, whereas the predicted PTI rank was 32 that was relatively uniform across the peninsula. This discrepancy may attribute to the site's localized topographic conditions, which may not be adequately represented by the spatial resolution of satellite open data in this study.

Overall, these three stations demonstrated that local environmental conditions can substantially influence the PTI rankings. Additionally, where trends were detected, the satellite-based MAGT trends consistently indicated warming across the study region, in agreement with the widespread permafrost warming observed globally (Biskaborn et al., 2019). However, limited studies have suggested that high-elevation permafrost may exhibit short-term cooling trends driven by local factors such as snow and topography (Luetschg et al., 2008). Among the 96 stations examined in this study, a few sites also exhibited weak decreasing MAGT trends. Future studies incorporating finer-scale local environmental variables may help explain these site-specific MAGT trends and improve the representation of local permafrost conditions."

(3) Finally, in the Discussion section, "3.4 Satellite-based open data for permafrost research", we further addressed uncertainties in satellite datasets by adding the following statements.

"…However, XGBoost is a data-driven algorithm. Rather than explicitly solving equations governing heat transfer, hydrological processes, or soil freezing/thawing, its extrapolation capability depends on the environmental conditions represented by the explanatory variables in training samples. Its predictive performance may decrease when the explanatory variables are not sufficiently representative, or when the training dataset inadequately captures the complex and heterogeneous environments such as sporadic permafrost, and isolated patches, and alpine permafrost zones…"

> *"…While different modelling approaches have been incorporated into the three permafrost products (Obu, NIEER, and Permafrost_CCI) used in this study, all three products rely heavily on thermal characteristics of satellite observations (e.g., MODIS) and ERA5 climate reanalysis. Therefore, they may share common biases in estimating permafrost conditions of PP, MAGT and ALT. Substantial discrepancies were observed among these products, and this study sought to reduce the product-specific uncertainties by generating an ensemble layer of permafrost conditions. Yet common biases among the three satellite-based products remain and could propagate into the derived PTI layer. An outstanding example is peatland permafrost. Along the coastline of Quebec-Labrador Peninsula, Canada, Wang et al. (2023b) documented the presence of permafrost complexes associated with palsa bogs and peat plateaus. Way and Lewkowicz (2016) developed a snow-modified TTOP map that revealed more heterogeneous permafrost distributions after accounting for localized variability in geomorphology and snow cover in peatlands. More specifically, Way et al. (2018) identified a uniquely large thermal offset in peatland permafrost regimes, indicating greater resilience than suggested by existing permafrost maps. In this study, we compared ground temperatures from four borehole sites at Ungava Bay with our ensemble estimates. The ensemble MAGT was consistently higher at these sites, resulting in an underrepresentation of permafrost stability along the Labrador coastline. Global peat datasets remain limited and available only at coarse resolutions. Moreover, coastal peatland permafrost is often narrow and limited in spatial extent and therefore, cannot be effectively distinguished in existing global products."*

Please also refer to our response to Comment #3 regarding new, finer-scale satellite datasets.

2. Obu vs Westermann et al.:

Treating the two data sets as equal in the process of building the ensemble data set is a mistake in my opinion. These are not merely two existing data sets but, in many ways, one is the successor to the other. Westermann et al., does not only provide time series, an advantage over the Obu et al. publication, it also employs a more sophisticated model. Please refer to the current data set and citation for more information:

Westermann, S.; Barboux, C.; Bartsch, A.; Delaloye, R.; Grosse, G.; Heim, B.; Hugelius, G.; Irrgang, A.; Kääb, A.M.; Matthes, H.; Nitze, I.; Pellet, C.; Seifert, F.M.; Strozzi, T.; Wegmüller, U.; Wieczorek, M.; Wiesmann, A. (2025): ESA Permafrost Climate Change Initiative (Permafrost_cci): Permafrost version 4 data products. NERC EDS Centre for Environmental Data Analysis, *date of citation*. https://catalogue.ceda.ac.uk/uuid/c116848868054e18a9f5a51d68c3ad21

Westermann, S., Ingeman-Nielsen, T., Scheer, J., Aalstad, K., Aga, J., Chaudhary, N., Etzelmüller, B., Filhol, S., Kääb, A., Renette, C., Schmidt, L. S., Schuler, T. V., Zweigel, R. B., Martin, L., Morard, S., Ben-Asher, M., Angelopoulos, M., Boike, J., Groenke, B., Miesner, F., Nitzbon, J., Overduin, P., Stuenzi, S. M., and Langer, M.: The CryoGrid community model (version 1.0) – a multi-physics toolbox for climate-driven simulations in the terrestrial cryosphere, Geosci. Model Dev., 16, 2607–2647, 2023. https://doi.org/10.5194/gmd-16-2607-2023.

Thank you for sharing these two references. We have cited the first reference (Westermann et al. 2024) in the original manuscript. We double checked the web link and confirmed that version 4 of the dataset was released in 2024. In our description of the Permafrost_CCI product, we added information about permafrost model (CryoGrid) and cited the second reference (Westermann et al. 2023).

Among the three permafrost products used in this study, the Obu product was published first, in 2019, and was cited by both the NEERI (2022) and Permafrost_CCI (2024) products. As you mentioned, the Permafrost_CCI product did not adopt the TTOP approach developed by Obu et al. (2019). Instead, it employed a ground thermal model, CryoGrid, to derive permafrost variables.

In **Subsection 2.1.1 "Permafrost maps"**, we revised the descriptions to better reflect their methodological differences.

> *"…The Obu product includes two static layers: mean annual ground temperature (MAGT) at the depth of zero annual amplitude, and permafrost fraction (%) with MAGT below 0 °C within each 1 × 1 km^2 pixel. The latter is derived from an ensemble of 200 TTOP model realizations spanning a range of land-surface and thermal conditions to account for subpixel heterogeneity."*

> *"…The (NIEER) product is derived as the ensemble means of four statistical, machine learning and deep learning models, with each model going over 1,000 runs of resampled training dataset. The dataset includes three static layers: MAGT, active layer thickness (ALT), and permafrost fraction (%), also calculated as the probability across the ensemble model realizations."*

> *"…For the Permafrost_CCI product, an ensemble ground thermal model (CryoGrid) numerically solves the heat conduction equation within the thermal profile from ground surface downwards (Westermann et al. 2023). The Permafrost_CCI maps include annual layers of MAGT, ALT, and permafrost fraction (%) that is calculated as the in-pixel probability of permafrost existence averaged across simulations from seven ensemble model members. Consequently, the permafrost fraction data contains seven discrete values ranging from 14% (1/7) to 100%."*

3. Landcover and DEM:

Arctic landcover, specifically tundra, is often misrepresented in global landcover mapping efforts. Therefor using these data sets to establish an ensemble data set for permafrost regions may lead to mischaracterization in analysis building on the ensemble data. The CAVM data set, while being a well-respected and great data set for Arctic tundra, vegetation suffers from coarse spatial resolution and possible underestimation of certain landcover types due to this. I advise the authors to do additional literature research regarding available Arctic landcover and existing synthesis efforts e.g:

Bartsch, A., Efimova, A., Widhalm, B., Muri, X., von Baeckmann, C., Bergstedt, H., Ermokhina, K., Hugelius, G., Heim, B., and Leibman, M.: Circumarctic land cover diversity considering wetness gradients, Hydrol. Earth Syst. Sci., 28, 2421–2481, https://doi.org/10.5194/hess-28-2421-2024, 2024.

Briones, V., Genet, H., Jafarov, E., Rogers, B., Watts, J., Virkkala, A.-M., Bartsch, A., Maglio, B., Rady, J., and Natali, S.: Fusing Local and Regional Datasets to Develop a Composite Land Cover Product Across High Latitudes, Earth Syst. Sci. Data Discuss. [preprint], https://doi.org/10.5194/essd-2026-29, in review, 2026.

DEM: Instead of combining different sources, why not use the Copernicus DEM, available for the entire region.

https://dataspace.copernicus.eu/explore-data/data-collections/copernicus-contributing-missions/collections-description/COP-DEM

Thank you for these new references. We combine your comments regarding land cover and DEM in this response. The CALU product (Bartsch et al., 2024) and the Copernicus DEM product (ESA, 2024) are now cited and discussed in the revised manuscript. The study by Briones et al. could provide a valuable resource for future studies. Because it is currently under review, we have decided not to cite it at this stage.

The Circumarctic Land Cover Units (CALU) dataset by Bartsch et al. (2024) has an impressive spatial resolution of 10 m derived from Sentinel-1 and Sentinel-2 imagery. It enables much finer-scale land cover delineation in wetlands and moist tundra. Our study, however, was conducted at the kilometer scale, and the land cover map used in our analysis covers both the Circumarctic region and other high latitudes. Therefore, we made substantial efforts to integrate multiple land cover maps with comparable spatial resolutions together. Our ensemble land cover map has been released on Zenodo.

The study by Briones et al. (in review) has an objective similar to that of our land cover ensemble effort, as both integrate multiple existing global and regional land cover datasets. The Briones study incorporates a broader range of datasets within a machine learning framework. Its methodological design is more rigorous than our expert knowledge-based approach. Once published, the dataset by Briones study will be valuable for many applications across thee northern high latitudes, including our future research in this aspect.

Regarding the DEM dataset, we appreciate learning about the high-resolution, global Copernicus DEM products (GLO-30 and GLO-90), which have spatial resolutions of 30 m and 90 m, respectively. However, our study was conducted at the kilometer scale. The DEM dataset we obtained from WorldClim is readily available at this resolution, and it has integrated different sources to provide global coverage. Therefore, we used the WorldClim DEM for simplicity and consistency with the spatial scale of our analysis.

We revised Subsection "**3.4 Satellite-based open data for permafrost research**" in the **Discussion** section to cite these new sources and discuss the broader impact of open satellite data. A new paragraph was added:

> *"Recent advances in big data analytics and geospatial data science have accelerated the production of open satellite datasets at finer resolutions and across larger geographic extents. For example, the Copernicus DEM products GLO-30 and GLO-90, derived from the twin TerraSAR-X and TanDEM-X satellite observations between 2011 and 2015, provide global surface elevation data at spatial resolutions of 30 m and 90 m, respectively (ESA, 2024b). Unlike conventional digital terrain model products, the Copernicus DEM represents the Earth's top-reflective surface, including buildings, infrastructure and vegetation; therefore, it captures land-surface characteristics beyond elevation alone. Derived from Sentinel-1 radar and Sentinel-2 multispectral imagery acquired over a seven-year period from 2016 to 2022, the Circumarctic Land Cover Units (CALU) delineates heterogeneous land covers in the Arctic at 10 m resolution, enabling improved representation of arctic wetlands and moist tundra (Bartsch et al., 2024). As increasingly detailed spatial data products become available, future applications will benefit from their enhanced environmental characterization and support for localized permafrost modelling, helping researchers better identify, interpret and mitigate common uncertainties in satellite-derived datasets."*